JAMES A. ST. VILLE, JOHN A. ECKER, JAMES M. WINGET, AND MERI H. BERGHAUER

THE ANATOMY OF MIDTHIGH PAIN AFTER TOTAL HIP ARTHROPLASTY

A study was conducted to determine the probable sources of midthigh pain following human total hip joint replacement surgery (arthroplasty) using uncemented prostheses. Standard finite-element analysis techniques are used to determine the implications of several clinical situations. Stem length, implant material, and loading conditions are examined, and the results are correlated to various laboratory and clinical findings. A cascade chart, based on changes in the stress and strain environment within the femur after total hip arthroplasty, details the physiologic events that result in midthigh pain.

OVERVIEW

Midthigh pain is an iatrogenic problem (i.e., an inadvertent effect of treatment) that has developed with the advent of total hip arthroplasty, the surgical procedure in which affected bone of the femur is resected and a prosthesis is inserted into the resulting cavity. The implant device may be secured with bone cement or, increasingly, by using a press-fit without cement (Fig. 1). Midthigh pain is more common in uncemented femoral components than in cemented implants and can last two years or longer. Midthigh pain appears more frequently in very active patients; correlative relationships to sex and bone quality have not yet been determined. Classic midthigh pain is described as a dull, aching sensation, often worsening with such activities as climbing stairs and rising from a chair. The etiology of this pain is not adequately understood, but it is perceived to be related to the stiffness mismatch between the bone and the implant material.

This study closely explores the stress/strain relationships in the femoral diaphysis (shaft) at the tip of the femoral component under various clinical situations: different loading conditions, stem lengths, and implant material properties. In addition, this report introduces a new scientific method of interactive volumetric rendering of finite-element data, a display technique that enables visualization of three-dimensional spatial location and orientation of stress isosurfaces. Interactive manipulation of these isosurfaces makes possible easy correlation with previous clinical, radiographic, laboratory, and nuclear medicine findings. Using this technique, stress type (principal stresses, stress intensity, Hencky–von Mises stresses), stress magnitude, area of distribution, and orientation of stress isosurfaces can be displayed and controlled in real time.

The cortex (outer layer of hard bone responsible for strength and stiffness of the femur) and the cancellous bone (soft inner core of the femur structure, commonly referred to as bone marrow) were mathematically modeled. An uncemented, collarless, press-fit femoral component was modeled within the femur under eight different clinical situations. The first group consisted of a cobalt–chromium alloy femoral component with three different stem lengths: short (117 mm), standard (132 mm), and long (147 mm). The second group consisted of a standard-length femoral component made of three different materials: cobalt–chromium alloy, titanium alloy, and polysulfone composite. The third group simulated a standard-length cobalt–chromium stem subjected to one-leg stance (normal walking gait) and midrise (getting out of a chair) loading conditions.

Increasing stem length tended to increase both stress distribution and magnitude in the cancellous bone, just proximal to the stem tip on both the axial tension and compression sides. All models, regardless of stem length, had peak cortical stress isosurfaces at or slightly distal to the level of the stem tip. At 90° to the peak cortical stress isosurfaces, the cortical stresses approached zero, representing the transition point from tensile to compressive stresses (neutral stress plane).

The effects of different material properties demonstrated similar patterns of cortical stress distributions for the cobalt–chromium alloy and the titanium alloy. The cobalt–chromium alloy had slightly higher endosteal (i.e., located within the cancellous bone) stress magnitudes, whereas the peak cortical stress magnitudes were essentially the same. In comparison with the two metals, the polysulfone composite implant had unique endosteal and cortical loading distributions and magnitudes. Loading distribution appeared to be homogeneous throughout the cortical and endosteal layers, without separate areas of peak cortical and peak endosteal magnitudes. The polysulfone composite implant allows a more uniform stress transfer distributed over larger cortical and endosteal areas when compared with either of the metal implants.

The variable loading condition study demonstrated similar stress patterns in the one-leg stance and midrise. Variations between these two loading situations were in

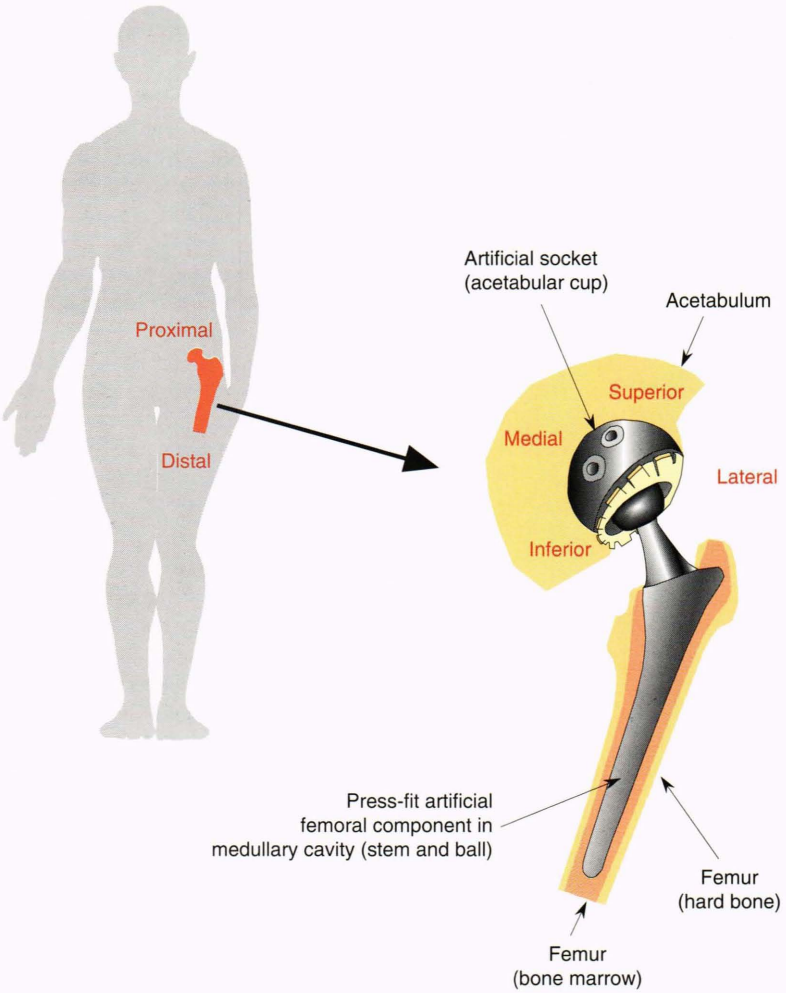

Figure 1. Representative anatomy of a total hip arthroplasty showing resected femur with a press-fit (uncemented) femoral prosthesis and an artificial acetabular cup. Terms in red are directional indicators. Anterior (front) and posterior (rear) are not shown.

the magnitudes of peak Hencky–von Mises stresses and the orientation of both the stress isosurfaces and the neutral stress plane. Hencky–von Mises stress describes a multiaxial stress state using a single value. The associated theory (also referred to as the maximum distortion energy theory) presents a criterion for predicting ductile yielding using the Hencky–von Mises stress of the combined loading. The Hencky–von Mises failure criterion is commonly accepted as a plasticity flow rule and is recognized for its accurate prediction of ductile failure. In midrise, the peak cortical and endosteal magnitudes are much greater, reflecting the higher pressures on the femoral head that result from the act of getting out of a chair. The orientation of midrise peak stress magnitudes is about 90° (rotated about the long axis of the femur) to the orientation of one-leg-stance peak stresses. This study clearly demonstrates that peak cortical stresses migrate along the cortex surface and that peak endosteal stresses migrate within the cancellous bone, corresponding to a concurrent orientation change of the neutral stress plane within the femoral component stem.

Patterns of stress isosurfaces at the femoral stem correlate with reported radiographic bone remodeling changes of cortical thickening[1] and endosteal consolidation.[2] The orientation and magnitudes of these stresses are such that both cortical and cancellous bone remodeling would be expected.[3–6] Additionally, the predicted stresses are great enough to cause bone microfractures.[7–9]

The presence of any femoral prosthesis in the medullary cavity may increase the effective stiffness of the proximal femur (near the hip joint). Stresses generated by this stiffness mismatch result in localized areas of microfractures, localized stem micromotion, and zones of stress-induced bone remodeling in the cortical and cancellous bone. The unmyelinated type-C nerve fibers accompanying the blood vessels in the osteon (the "living" organ of the bone) and the trabecular (cancellous) bone may be subjected to these localized changes of stretch and pressure, resulting in the classic dull, aching sensation that is characteristic of midthigh pain.[10,11] The pain presumably continues until bone remodeling is completed and a new bone ultrastructure is formed to accommodate this unphysiological stiffness mismatch.

INTRODUCTION

Total hip arthroplasty began in 1958, when Sir John Charnley implanted the first artificial hip in a human.[12] Some 120,000 total hip arthroplasties are now performed

each year in the United States. Over the past three decades, femoral component design rationale has continuously changed to address various clinical problems that have evolved from the previous generation of total hip designs. Initial designs had relatively short stems with small cross-sectional areas, and usually they were cemented in the femur (Fig. 2A). Frequent implant fatigue failures and loosening at the bone-to-cement interface resulted in new prosthesis designs, including longer stems with larger cross-sectional areas, uncemented prostheses, and porous surface coatings (for bone ingrowth) (Fig. 2B).[13]

Over the past seven years, the incidence of midthigh pain associated with uncemented femoral total hip replacements has increased worldwide (T. A. Gruen, personal communication, 1989).[14–18] Patients with high activity levels, namely younger patients and active older patients, are most likely to experience problems. It is not well understood to what degree midthigh pain correlates with the stress/strain relationships at the femoral component tip that result from unphysiological bone-to-implant stress mismatch. Nonetheless, clinical findings of increased pain resulting from high loading activities, such as stair-climbing and getting out of a chair, indicate that an association does in fact exist.

The pain often resolves over a two-year postoperative period but occasionally persists longer. Bone is essentially a natural, living, composite material capable of adapting to changes in its loading environment by remodeling its internal structure to produce different mechanical properties (stiffness, strength, and orientation of reinforcing fibers). Engh[1] described three clinical phases associated with bone remodeling and midthigh pain. The acute or traumatic phase (0–3 months) results in development of microfractures and subsequent fracture callus formation. During the adaptive phase (3 months to 2 years), bone reacts to the new stress fields and undergoes bone remodeling in accordance with Wolff's predictions. During the stable phase (more than two years), bone remodeling is static and the bone/implant structure is in dynamic equilibrium.[1] Clinically, midthigh pain appears to cease with the beginning of the stable phase.

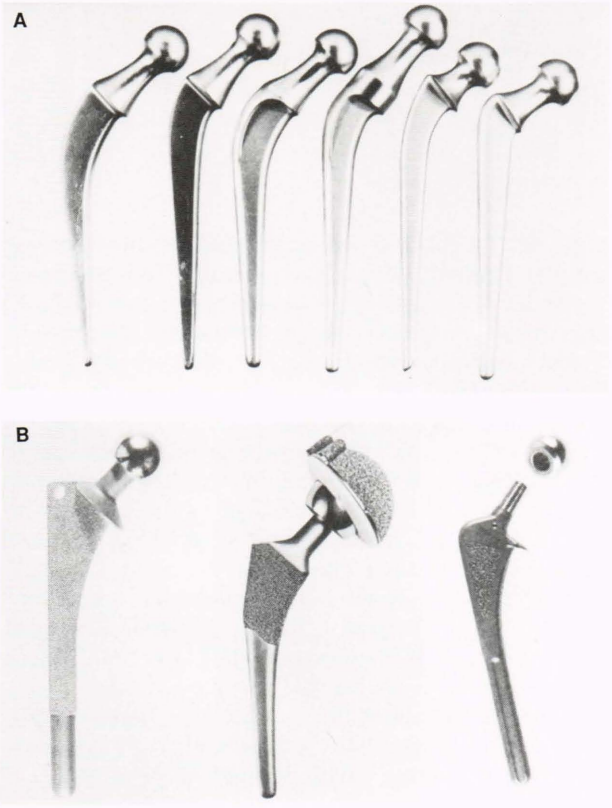

Figure 2. Examples of femoral prostheses used in total hip arthroplasty. **A**. Earlier Charnley (cemented) implants with characteristic short, slender femoral stems. **B**. Newer implant designs (cemented and uncemented) with thicker femoral stems and novel fixation techniques. (Reprinted, with permission, from Ref. 13.)

This article describes a representative mathematical model of an uncemented, collarless, press-fit total hip replacement. The predicted stress/strain relationships in the cortical and cancellous bone at the tip of the femoral component are examined under various clinical situations: three different lengths of stems, three different material properties, and two different loading conditions (one-leg stance and midrise).

An innovative computer visualization technique was developed for interactive volumetric rendering of finite-element data and analytical comparisons. The technique correlated the results of this study with clinical, radiographic, laboratory, and nuclear medicine findings to substantiate the cascade chart of physiological changes that result in midthigh pain.

MODEL DESCRIPTION AND LIMITATIONS

A three-dimensional finite-element model of a total hip arthroplasty was developed to understand the relationship of stress distribution, magnitude, and orientation to midthigh pain. The usefulness of such a model depends on its ability to characterize real clinical issues while minimizing the number and degree of the mathematical approximations. The goal of this project was to develop a "representative" mathematical model of an artificial hip replacement that reliably predicts stress trends adjacent to the femoral stem. Correlation of the results of this study with test results is considered later (see Discussion).

A linear finite-element analysis was performed assuming perfect connectivity (i.e., a well-bonded interface) between nodes at the cortical-to-cancellous bone interface and the cancellous-to-implant interface. The model consisted of 5207 nodes and 5040 isoparametric solid elements. Both hexahedronal and pentahedronal elements were used to ensure accurate shape adherence with the computed tomography (CT) geometry data (Fig. 3). The cortical bone was modeled as transversely isotropic (elastic modulus [E] = 11.0 to 17.0 Gigapascals [GPa], shear modulus [G] = 4.0 to 6.0 GPa, Poissons ratio [ν] = 0.30 to 0.37, and density [ρ] = 2.0 g/cm^3). The nonlinear anisotropic cancellous bone has mechanical properties that depend on the location and quality of bone; therefore, approximate values (E = 0.30 to 0.60 GPa, G = 0.13 to 0.20 GPa, ν = 0.32 to 0.35, and ρ = 0.50 to 0.70 g/cm^3) were determined after reviewing

Table 1. Material properties of bone and implants.

Property	Bone type		Implant type		
	Cortical	Cancellous	Co–Cr–Mo	Titanium alloy	Polysulfone (30% carbon-filled)
Elastic modulus, E (GPa)	11.0–17.0	0.30–0.60	214.0	110.0	10.5
Shear modulus, G (GPa)	4.0–6.0	0.13–0.20	82.3	41.4	4.4
Poisson's ratio, ν	0.30–0.37	0.32–0.35	0.30	0.33	0.20
Density, ρ (g/cm^3)	2.0	0.50–0.70	7.86	4.43	1.37

Note: Co–Cr–Mo is the cobalt–chromium alloy.

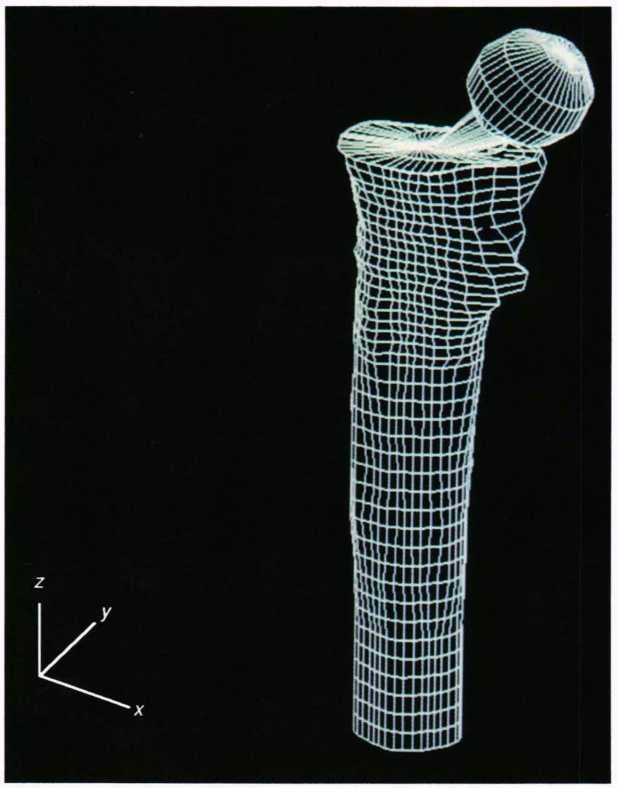

Figure 3. Total hip arthroplasty, fine-mesh model, as generated from computed tomography scan data (5207 modes, 5040 elements).

the works of Amtmann, Cezayirlioglu, Evans, Knauss, Lappi, Vichnin, and others (Table 1).[19–27]

To understand the effect of stem length on tip stress, three cobalt–chromium alloy stems of different lengths (117 mm, 132 mm, 147 mm) were modeled, all with a tip diameter of 12.25 mm. Three different implant materials were examined for effects on the stress/strain distribution within the femur. Two metal alloys, cobalt–chromium (E = 214.0 GPa, G = 82.3 GPa, ν = 0.3, ρ = 7.86 g/cm^3) and titanium (E = 110.0 GPa, G = 41.4 GPa, ν = 0.33, ρ = 4.43 g/cm^3), were modeled as isotropic materials. A linear homogeneous polysulfone (30% carbon-fiber–filled) composite (E = 10.5 GPa, G = 4.4 GPa, ν = 0.20, ρ = 1.37 g/cm^3) was modeled to evaluate the effects of substantially reducing the implant stiffness (Table 1). Two different pressure loads, simulating walking and rising from a chair, were analyzed. Pressure distributions and magnitudes applied to the femoral head were based on *in vivo* studies.[28] The resultant force of each of these pressures was approximately 2,000 Newtons (N), with an orientation change from one-leg stance to midrise loading (Fig. 4).[28–33] To avoid rigid body motion and to support the applied load, the distal end of the femur was subjected to a fixed displacement boundary condition.

This project, like all finite-element studies, introduces approximations because it is not possible to model all the nonlinearities and variabilities in biologic tissues.[34–38] As a result, the reader should be aware of the limitations or inaccuracies introduced by these mathematical models. In finite-element modeling of biologic tissues, however, emphasis should be placed not on absolute results, but on the relative trends of magnitudes, distributions, and orientations. If more precise values are sought, more detailed modeling should be performed using an even finer finite-element mesh and redefinition of boundary conditions to minimize inaccuracies in the area of interest.

MATERIALS AND METHODS

Specimen Preparation

Cadaveric femurs were harvested and debrided of soft tissue. The femoral necks were cut in a surgical fashion, and uncemented, collarless, press-fit femoral components were introduced into the medullary cavities. These femurs, with implants, were subjected to CT scanning. For continuity of modeling and ease of comparison, a single femur was used throughout this project.

Computed Tomography

The femurs were X-rayed using either a Siemens Somatom DR3 or a GE 9800 CT scanner. The scans extended

from the isthmus of the femur to the proximal head and neck of the implant. The CT examination consisted of thirty-five to forty-five overlapping transaxial scans, and scanning parameters were characteristic of the scanner used. A two-dimensional (cross-sectional) image of each of the slices was created after an analog-to-digital conversion. Final signal processing was performed using a DEC PDP/11 computer system. Transparent hardcopy films were created, and the image data were transferred to magnetic tape (Fig. 5).

Preprocessing of Data

The individual image data slices were read from the magnetic tape and converted to PDA-PATRAN (PDA Engineering) finite-element preprocessing formats. For the two-dimensional image data, PDA-PATRAN software was used in the discretization (differentiation) of bone type (cortical and cancellous) and implant material. Nodal points were created at the boundaries of the different structured layers (cortical bone, cancellous bone, and implant surface). Forty nodal points were created around the circumference of each of the boundaries, similar to Saejong et al., for continuity of model design and ease of comparison.[39,40] The two-dimensional image data arrays were properly oriented to develop a three-dimensional arrangement of the nodal points.[41] Isoparametric solid elements were then created to provide connectivity between the nodes. A standard 32-mm-diameter femoral head was modeled at the end of the implant stem to provide an appropriate loading base.

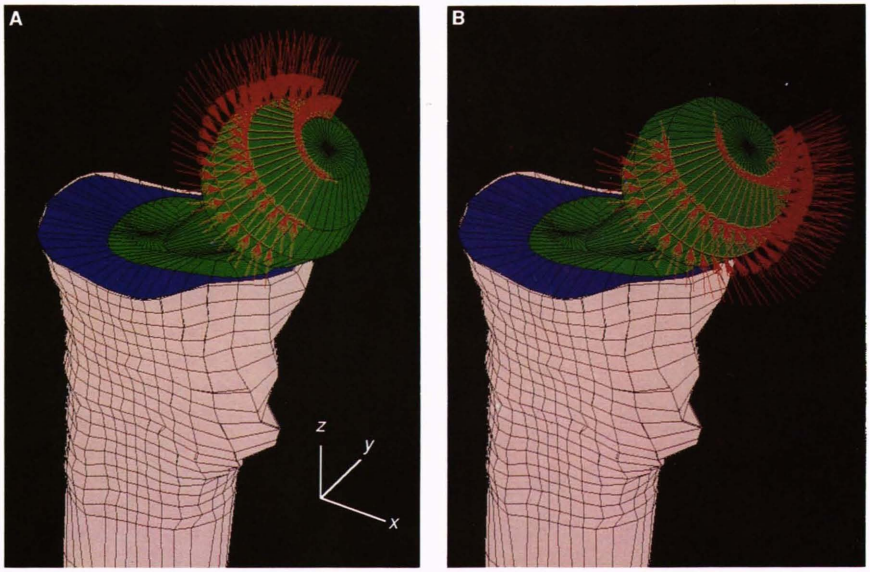

Figure 4. Computer representation of approximate pressure distribution and magnitude. Arrows indicate applied pressure locations and correspond to approximate *in vivo* magnitudes. **A**. One-leg stance loading. **B**. Midrise loading.

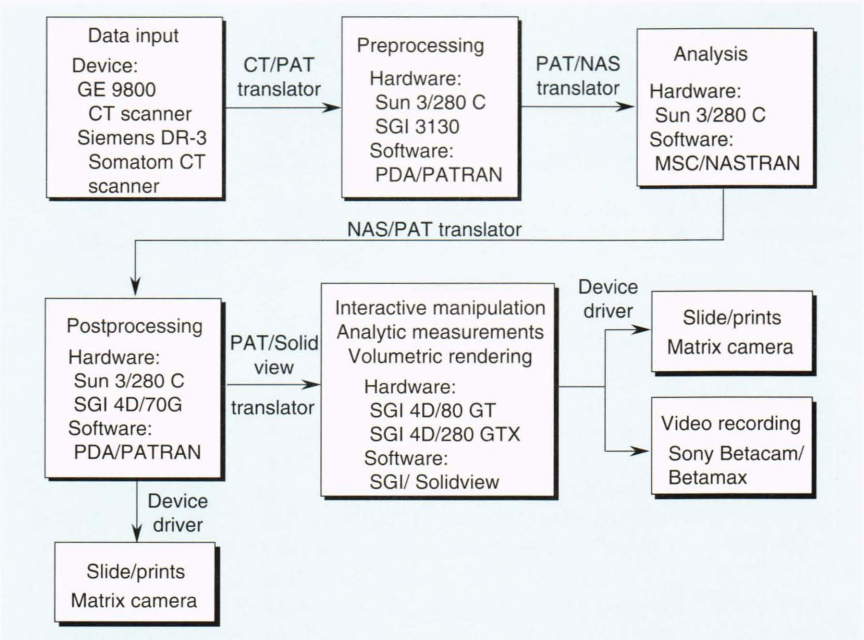

Figure 5. Flowchart of hardware devices, software, and analytical procedures used in this study.

The finite-element model consisted of more than 5000 isoparametric solid elements. Both hexahedronal (six-face) and pentahedronal (five-face) elements were used to ensure accurate shape adherence with the CT scan data. All preprocessing and model checkout computations were performed using PDA-PATRAN software on a Sun 3/280C workstation (Sun Microsystems) and/or an IRIS 3130 workstation (Silicon Graphics) (Fig. 5).

Finite-Element Analyses

Finite-element analyses were performed using the general-purpose MSC/NASTRAN (MacNeal-Schwendler Corporation) software package on the Sun 3/280C workstation. Input bulk data decks were created from PDA-PATRAN models using the PATNAS (PDA Engineering) translator, with some custom modifications. Various advanced capabilities of the MSC/NASTRAN software were employed to simplify analysis. Internal nodal resequencing and optimization were performed to reduce execution time and to retain compatibility among the different models. Checkpoint and restart capabilities were used to reduce formulation times of stiffness and mass matrices when only minor loading or boundary constraint changes occurred. Substructure (superelement) analysis techniques were used to partition the bone and the implant structures so as to conserve computational resources, thereby increasing solution efficiency (Fig. 5).

Postprocessing of Data

The results were output from the MSC/NASTRAN finite-element analyses for display and evaluation using the PDA-PATRAN software. Data on element stress and strain and nodal force and displacement were translated using the NASPAT (PDA Engineering) translator; nodal stress and strain results were also output for comparison purposes. Data on the color-coded contour and fringe plots of the stress and strain results were produced on the finite-element models using PDA-PATRAN postprocessing; displacement contours and deformed geometry plots were also created using this software. Postprocessing was performed on Silicon Graphics 4D/70G and Sun 3/280C workstations (Fig. 5).

Volumetric Rendering

Nodal stress and displacement data from PDA-PATRAN, combined with the original-model coordinate geometry and element connectivity, were transformed into formats compatible with the SGI/SOLIDVIEW program (Silicon Graphics). This software program can perform solid-surface shading (used for stress color-fringe analysis) and alpha-blending transparency (used for three-dimensional spatial comparison). Use of SGI/SOLIDVIEW enables interactive real-time manipulation of three-dimensional solid model databases, analytical measurements, and instantaneous display of stress distributions (principal stresses, stress intensities, and Hencky–von Mises stresses). The software also allows interactive highlighting of a specific range of magnitudes of the results being displayed.[42]

Both the model and the cutting plane can be rotated using SGI/SOLIDVIEW; the model can also be scaled and translated for more detailed analysis. For ease of comparison, a multiwindow option was developed to compare two or more clinical models simultaneously. This feature enables synchronized rotation of the models, interactive display of stress distributions, and use of a range of magnitudes in each window. Interactive manipulation, analytical measurements, and volumetric rendering were performed on Silicon Graphics 4D/80 GT and 4D/280 GTX workstations using the SGI/SOLIDVIEW software.[42]

RESULTS

Stem Length

Three different lengths of uncemented, collarless, press-fit, cobalt–chromium alloy prostheses were mathematically modeled: 117 mm (short), 132 mm (standard), and 147 mm (long). The diameter of the implant stem at the tip was approximately 12.25 mm. One-leg–stance loading conditions were applied to the femoral head, with pressure magnitudes and distribution based on the *in vivo* measurements by Hodge et al.[28] The boundary conditions at the various interfaces were described in a preceding section (Model Descriptions and Limitations).

Maximum Hencky–von Mises stresses for the short stem were 169 megapascals (MPa) cortical, 98.7 MPa cancellous, and 98.7 MPa for the implant. Maximum stresses for the standard stem were 168.3 MPa cortical, 127 MPa cancellous, and 127 MPa for the implant. Finally, maximum stresses for the long stem were 154 MPa cortical, 164 MPa cancellous, and 164 MPa for the implant. The peak cortical stress value for the long stem is probably lower than indicated here, because of the proximity of the femoral component tip to the constrained end of the femur model (Table 2) (Fig. 6).

The locations of these peak stress isocontours vary. Peak cortical stresses appeared at, or slightly distal to, the level of the stem tip; peak endosteal stresses appeared proximal to the implant tip. Distinct areas of peak cortical and peak endosteal stresses on both the lateral and medial sides corresponded to the areas of axial tension and compression. Approximately 90° (rotated about the long axis of the femur) to the peak cortical and endosteal stresses is a vertical plane where the stresses approach

Table 2. Maximum Hencky–von Mises stresses (MPa) with different implant materials, load sets, and stem lengths.

	Bone type		
Implant material	Cortical	Cancellous	Implant
Co–Cr–Mo (cobalt–chromium alloy)			
Load set[a]			
One-legged stance	168.3	127.0	127.0
Midstance or midrise	258.0	191.0	191.0
Stem length (mm)			
Short (117)	169.0	98.7	98.7
Standard (132)	168.3	127.0	127.0
Long (147)	154.0	164.0	164.0
Titanium[a]	168.0	102.0	102.0
Polysulfone (30% carbon-filled)[a]	169.0	64.0	29.0

[a]Standard length (132 mm).

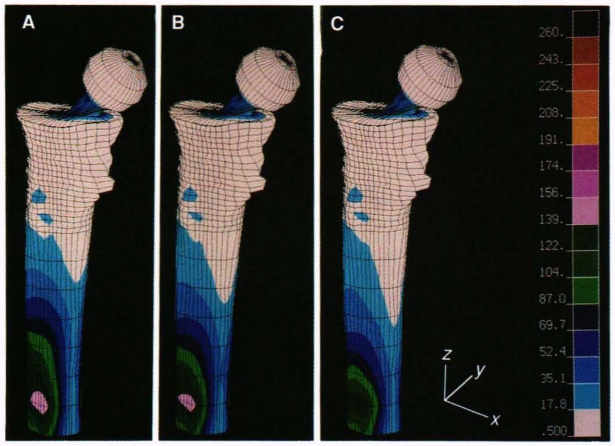

Figure 6. Hencky–von Mises stress (MPa) distributions along the cortical surface for three different stem lengths. **A**. Short, 117 mm. **B**. Standard, 132 mm. **C**. Long, 147 mm. Peak stresses for the long stem are probably lower than indicated because of the proximity of the stem tip to the fixed displacement boundary conditions of the distal femur.

zero (neutral stress plane) (Fig. 7). The neutral stress plane constantly rotates about the long axis of the femur because of fluctuating femoral head pressure magnitudes and pressure distributions under different loading conditions (e.g., walking, running, stair-climbing, and getting in and out of a chair). This neutral plane may also be constantly translating in the anterior/posterior or medial/lateral directions as a result of the cantilevering phenomenon existing within the complex geometry of the bone/implant structure.

Material Properties

Standard-length, uncemented, collarless, press-fit prostheses were mathematically modeled with three different material properties: cobalt–chromium alloy, titanium alloy, and polysulfone (30% carbon-fiber–filled) composite. Again, one-leg–stance loading conditions were applied from *in vivo* studies.[27] The boundary conditions for all three models remained unchanged from the previous models.

The maximum Hencky–von Mises stresses for the cobalt–chromium alloy stem were 168.3 MPa cortical, 127 MPa cancellous, and 127 MPa for the implant. The maximum stresses for the titanium alloy stem were 168 MPa cortical, 102 MPa cancellous, and 102 MPa for the implant. Finally, the maximum stresses for the polysulfone composite were 169 MPa cortical, 64 MPa cancellous, and 29 MPa for the implant (Table 2) (Fig. 8).

The cobalt–chromium alloy and titanium alloy implants have nearly identical patterns of stress isosurface formations. Both metals have two distinct areas of maximum cortical and maximum endosteal stress concentrations on both the medial (axial compression) and lateral (axial tension) sides. The composite has a unique distribution of stress concentrations. A maximum cortical concentration seems to exist, and decreasing-magnitude stress isosurfaces propagate in a homogeneous fashion throughout the cortical and cancellous layers. In addition, for a fixed range of stress magnitudes, the area of

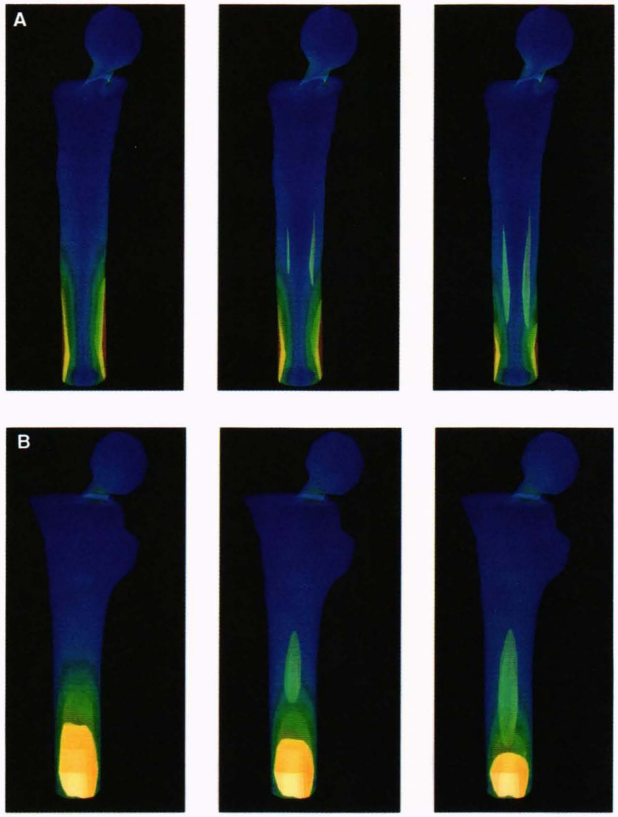

Figure 7. Three-dimensional alpha-blending transparency of Hencky–von Mises stress distributions. Three lengths of stems were modeled: short, 117 mm (left); standard, 132 mm (middle); and long, 147 mm (right). **A**. Internal stress isosurfaces. Note the pattern of distinct areas of cortical and cancellous stress concentrations. Magnitudes range from 0.0 MPa (blue) to 170.0 MPa (red). Highlighted stress isosurface magnitude range displayed is 100.0 MPa (green/yellow) to 170.0 MPa (red). **B**. Rotation enables visualization of the size and orientation of isosurface stress distributions.

distribution in the polysulfone is much larger than that in the two stiffer metals. This study clearly demonstrates the effects of substantially reducing material stiffness (i.e., reducing the elastic modulus, the shear modulus, the Poisson's ratio, and the density) (Fig. 9).

Loading Conditions

Two different loading conditions were applied to a standard-length, uncemented, collarless, press-fit cobalt–chromium alloy prosthesis, and the stress/strain relationships were mathematically predicted. The pressure magnitudes and distributions for both one-leg stance and midrise were based on *in vivo* measurements by Hodge et al.[28] The boundary conditions at the various interfaces were unchanged from the previous models.

The Hencky–von Mises stresses for one-leg stance were 168.3 MPa cortical, 127 MPa cancellous, and 127 MPa for the implant. The maximum stress magnitudes for midrise were 258 MPa cortical, 191 MPa cancellous, and 191 MPa for the implant (Table 2) (Fig. 10).

Changing loading conditions from one-leg stance to midrise created larger Hencky–von Mises stress magnitudes and caused reorientation of stress isosurfaces.

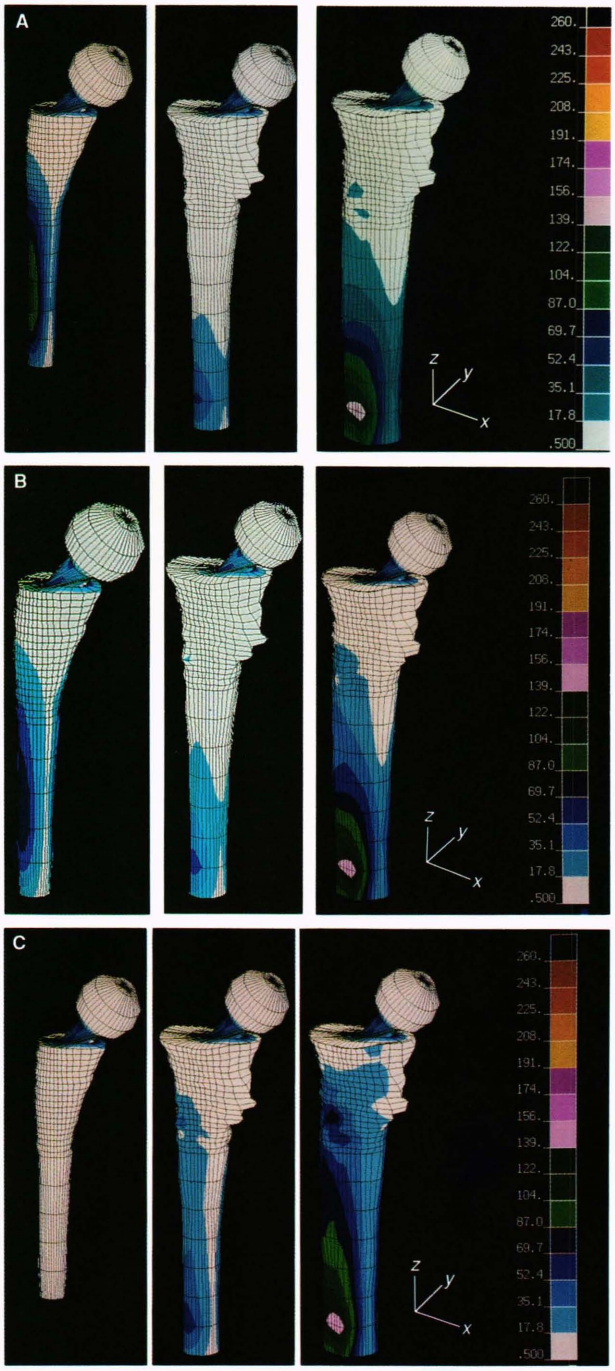

Figure 8. Color scales (MPa) showing Hencky–von Mises stress distributions. **A**. Cobalt–chromium alloy femoral component. **B**. Titanium alloy femoral component. **C**. Polysulfone (30% carbon-filled). For all three, the length of the implant was 132 mm. Stress distributions for each are shown at the implant surface (left), cancellous surface (middle), and cortical surface (right).

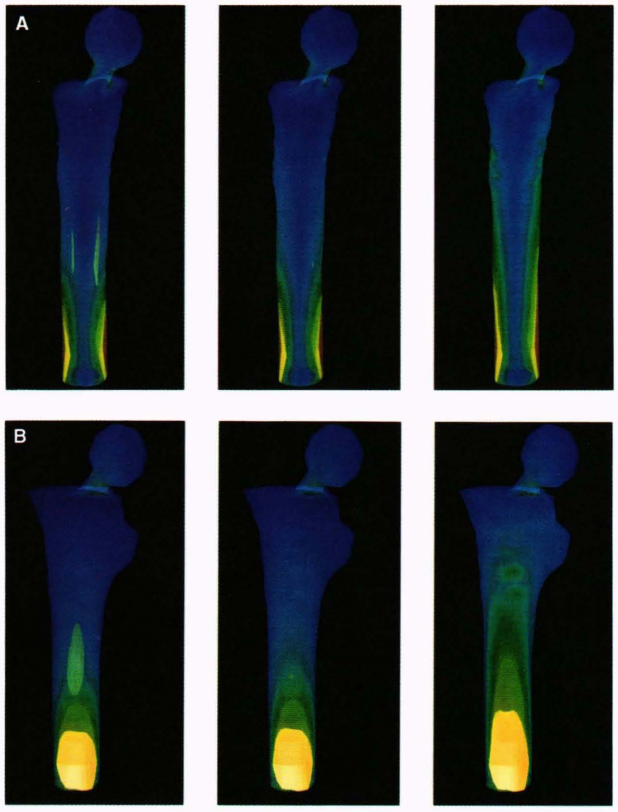

Figure 9. Hencky–von Mises stress isosurfaces for a 132-mm cobalt–chromium alloy stem (left), titanium alloy stem (middle), and polysulfone stem (right). **A**. Note the similar stress distribution pattern for the two metals; the composite has a more homogeneous stress distribution. Magnitudes range from 0.0 MPa (blue) to 170 MPa (red). Highlighted stress isosurface magnitude range displayed is 100 MPa (green/yellow) to 170 MPa (red). **B**. Rotation enables visualization of the size and orientation of the stress isosurface distribution for a given magnitude range.

The nearly 90-MPa increase in peak cortical stress and the 64-MPa increase in the peak cancellous stress reflect the effects of increased pressure magnitudes applied to the femoral head when the patient rises from a chair. Reorientation of the peak cortical and peak endosteal stresses (on both the axial tension and compression sides) reflects the different alignment of pressure distributions on the femoral head when subjected to midrise loading conditions (Fig. 11).

This study clearly demonstrates the significance of the theoretical neutral stress plane that exists within the femoral stem, representing the transition point from the tensile to compressive sides of the implant. The neutral plane rotates continuously about the long axis of the femur as a result of pressure distribution changes on the femoral head surface (walking, running, stair-climbing, and getting out of a chair). As the peak cortical and cancellous stress concentrations rotate, the orientation of the neutral stress plane follows. This factor is very significant in the design of the prosthesis and the bone/implant complex.

DISCUSSION

An extensive review of finite-element literature by Huiskes and Chao[36] emphasized the significance and limitations of mathematically modeling biologic tissue. Valuable information can be gained from representative models, despite known inherent inaccuracies. Previous

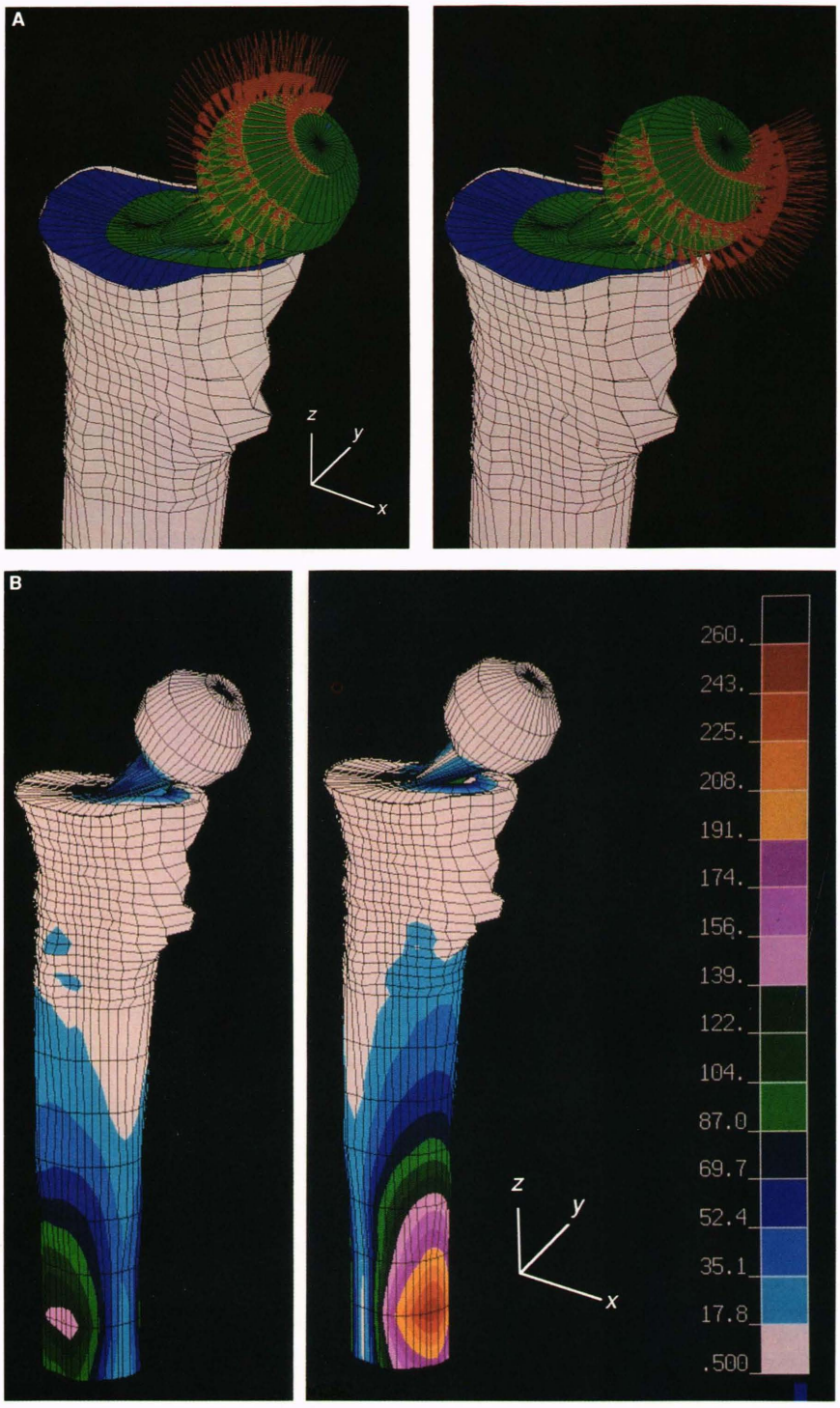

Figure 10. **A**. Computer representation of pressure magnitudes (MPa) and distribution for one-leg stance (left) and midrise (right). **B**. Hencky–von Mises stress (MPa) distributions at the cortical surface for a 132-mm cobalt–chromium alloy femoral component with one-leg–stance (left) and midrise (right) loading conditions. Note the change in orientation and magnitude of the peak cortical stress concentrations.

studies have focused on the modeling of cemented femoral components, whereas more recent analyses examined various uncemented clinical conditions and focused primarily on the stress/strain relationships of the proximal one-third of the implant, in particular the calcar region.[38,43–48] Our study specifically examines the region adjacent to the femoral stem tip, because unique adaptive bone remodeling has been reported in this area with uncemented total hip replacements.

Advances in both technology and finite-element mathematics have enhanced our ability to address the complexities inherent in biologic tissue modeling. Unfortunately, such studies can create as many questions as they answer. Our understanding of the local stress concentrations at the implant tip is just beginning. Future studies employing finer-mesh model generation, extended length, improved cancellous bone modeling, and additional dynamic loading conditions on the femoral head

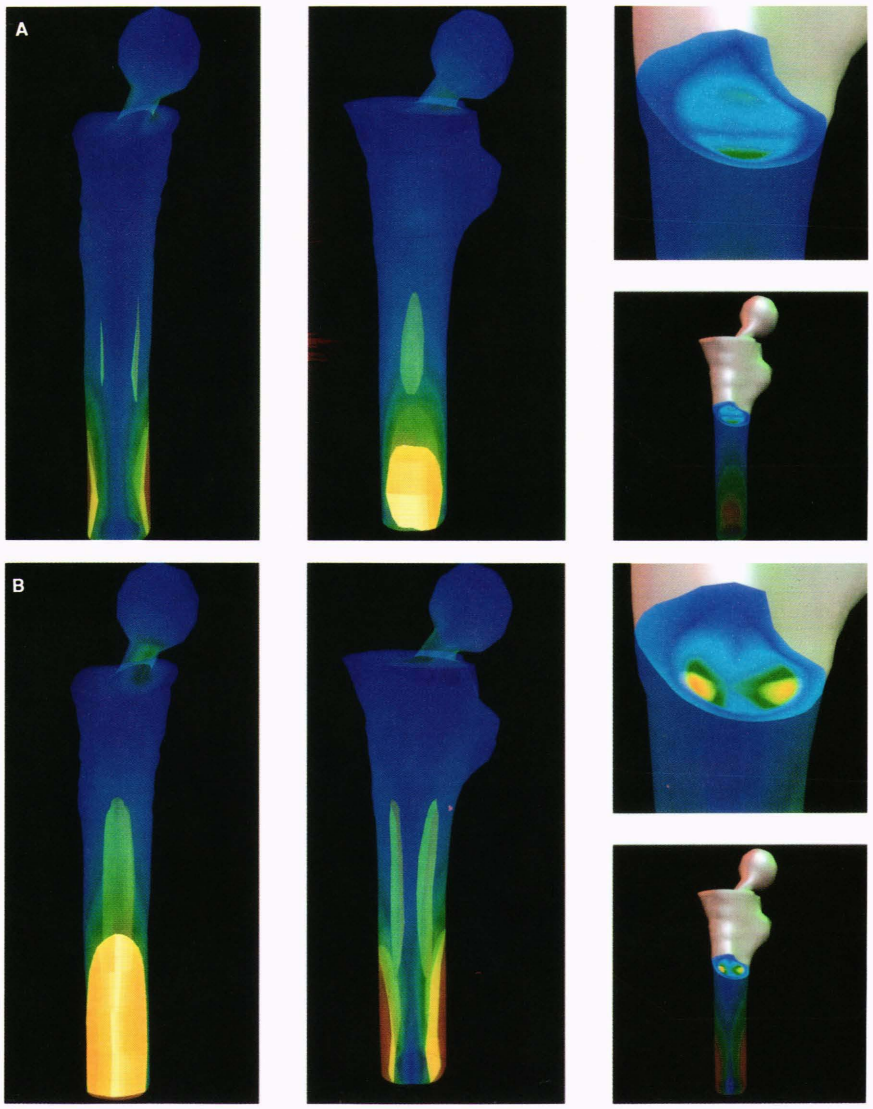

Figure 11. Hencky–von Mises stress isosurface distribution for a 132-mm cobalt–chromium alloy femoral component. **A**. Subjected to one-leg–stance loading conditions (left); rotated model (middle); blue horizontal neutral stress plane within implant (upper right) and its relationship to distal stress concentrations (lower right). **B**. Subjected to midrise loading conditions (left); rotated model (middle). Note the rotated blue vertical neutral stress plane within the implant (upper right) and its relationship to distal stress concentrations (lower right). Also note the increase in magnitude and change in stress orientation from A to B.

will provide more detailed information about total hip arthroplasty biomechanics.

The presence of a femoral component creates an unphysiological stiffness environment in the femur. The bone/implant structure is much stiffer than the original bone. As a result, the bone/implant structure undergoes a cantilevering phenomenon under physiological loads. Localized bending is well documented in photoelastic and strain-gauge studies.[49–51] Actual surface displacements for an implanted femur are much lower than those measured *in vitro* for an intact femur (Fig. 12).

Many recent strain-gauge and photoelastic studies have suggested the presence of a theoretical neutral stress plane between the tensile and compressive sides of the femur (Fig. 12).[49–52] Because those studies provide only surface displacement data, without providing much internal stress/strain information, three-dimensional mapping of this neutral plane is difficult. The volumetric rendering technique introduced in this study allows instantaneous scanning of a three-dimensional volume of data. Applying that technique to a three-dimensional finite-element database enables mapping of any stress type, magnitude, orientation, or area of distribution.[42]

The constantly changing position (rotation and translation) of the neutral stress plane in a normal femur may have an important role in future implant designs. If the bone/implant complex has a neutral stress plane that behaves in a manner similar to that of the neutral stress plane of an intact femur, then presumably the loads within the bone/implant complex will be distributed in a near-physiological fashion.

The apparent absence of midthigh pain reported during the first twenty-five years of total hip arthroplasty surgery suggests that the problem is iatrogenic and results from changes in the newer hip designs. Early designs had smaller cross-sectional areas and were cemented, whereas current designs have larger diameters and can be uncemented. Because stiffness increases with greater stem diameter, it is possible that the presence of a rigid implant in the medullary cavity causes a highly unusual load distribution in the bone. The presence of midthigh pain is well documented after *uncemented* total hip

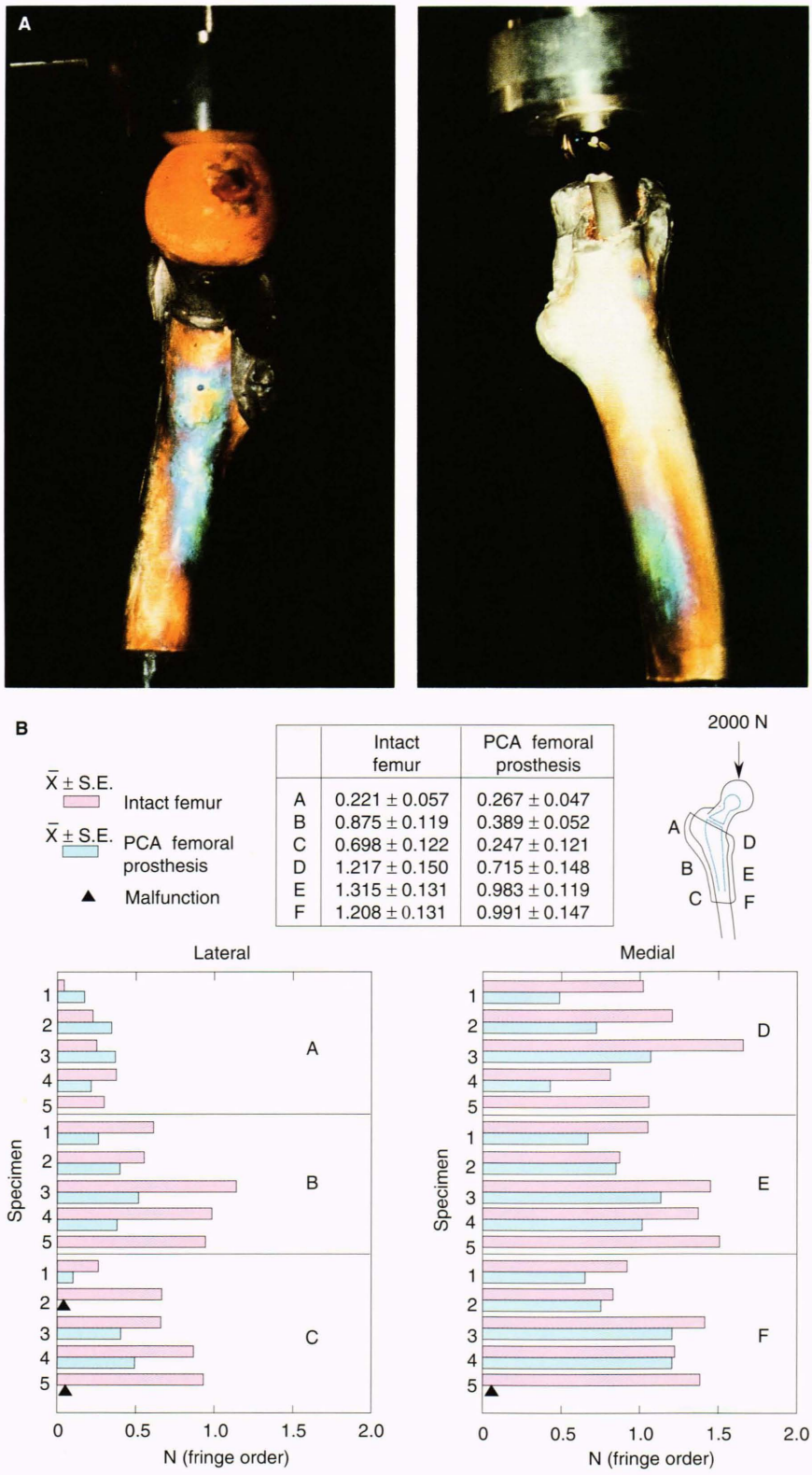

Figure 12. Strain comparison of intact versus implanted femur by photoelastic methods. **A**. Photoelastic strain pattern for intact femur (left) and implanted femur (right). Note that the presence of the implant stiffens the proximal femur, thereby reducing surface strain. **B**. Comparison of surface strains in stiffness of the proximal femur as a result of the presence of an implant. Fringe order (N) is a value determine through photoelastic studies and is directly proportional to the difference between the principal strains. PCA = porous-coated arthroplasty (uncemented implants from the Howmedica Company). (Reprinted, with permission, from Ref. 51.)

replacement. It remains to be seen, however, whether the incidence of midthigh pain will increase after *cemented* total hip replacement with the use of larger-diameter stems; early clinical and radiographic evidence indicate that this will occur (T. A. Gruen, personal communciation, 1989).[2]

The mechanical properties of an intact femur subjected to various physiological loading conditions have been defined using many different research modalities. Our project establishes a correlation between several clinical situations and their respective stress/strain effects on an implanted femur: the relationship between stem length

and load distribution in the cortical and cancellous layers; the relationship between change in the location of femoral head pressure distribution and reorientation of both the neutral stress plane and the area of peak stress concentrations; and, finally, the relationship between increased femoral head pressure magnitude and a corresponding increase in both peak cortical and cancellous magnitudes (near the implant tip).

Further, the cantilevering phenomenon of the bone/implant complex suggests concentrated bending of the bone layers adjacent to the implant tip. This bending is responsible for reorientation of the stress direction with increased radial compression (perpendicular to the long axis of the femur) on the axial tension side and increased radial tension on the axial compression side.

The physiological and mechanical responses to unusual loading conditions at the implant tip include bone remodeling, microfractures, and tip micromotion. Evidence of increased bone activity can be demonstrated with technetium scans (Fig. 13). Radiographic evidence shows that bone remodeling changes in this area consist of cortical hypertrophy and endosteal consolidation (Fig. 14). Studies by Wolff (1884), Roux (1895), and Kummer (1962) indicated that bone is "functionally" laid down in gross form, as well as in minute architecture, in accordance with the "maximum–minimum law" (maximum efficiency with minimum material).[3–5] Fyhrie and Carter noted the relationship of trabecular architecture to principal stress orientation. Endosteal consolidation conceivably is an example of trabecular reorientation (trajectory reorientation) in response to relatively high unphysiological radial forces.[6,53]

Although midthigh pain was believed to be related to an end-bearing stem within a tight intramedullary canal, several detailed radiographic and clinical studies of uncemented femoral total hip replacements were unable to confirm this relationship.[14,15,17] It was also postulated that midthigh pain may be caused by the transition of the stiffened proximal femur, as a result of the presence of an implant, to the more flexible femur below the tip of the stem.[16] A recently completed tri-institutional (Cleveland Clinic, Johns Hopkins Medical Institutions, and the Institute for Bone and Joint Disorders) five-year minimum radiographic follow-up of proximally porous-coated hip prostheses revealed a 51% incidence of cortical hypertrophy and a 58% incidence of endosteal consolidation (including 12% complete bridging below the tip). In this series, midthigh pain was seen in a few patients, usually within the first two years after surgery and often resolved thereafter. Precise information on the incidence and magnitude of midthigh pain was not sufficiently documented, because its specific nature was not recognized as a problem until years after the surgery (T. A. Gruen, personal communciation, 1989). That lack of precise documentation may account for inconclusive correlations of midthigh pain with radiographic bone remodeling changes in long-term clinical radiographic follow-up studies.

Despite the relatively high incidence of both endosteal consolidation and cortical hypertrophy, it is difficult to develop a staging or grading system of X-ray changes after total hip replacement (T. A. Gruen, personal communication, 1989). The observation that stress isosurfaces are constantly in motion, as a function of loading conditions, indicates that bone remodeling *must* occur and is distributed over areas of the cortical and cancellous bone layers. The location and size of the areas

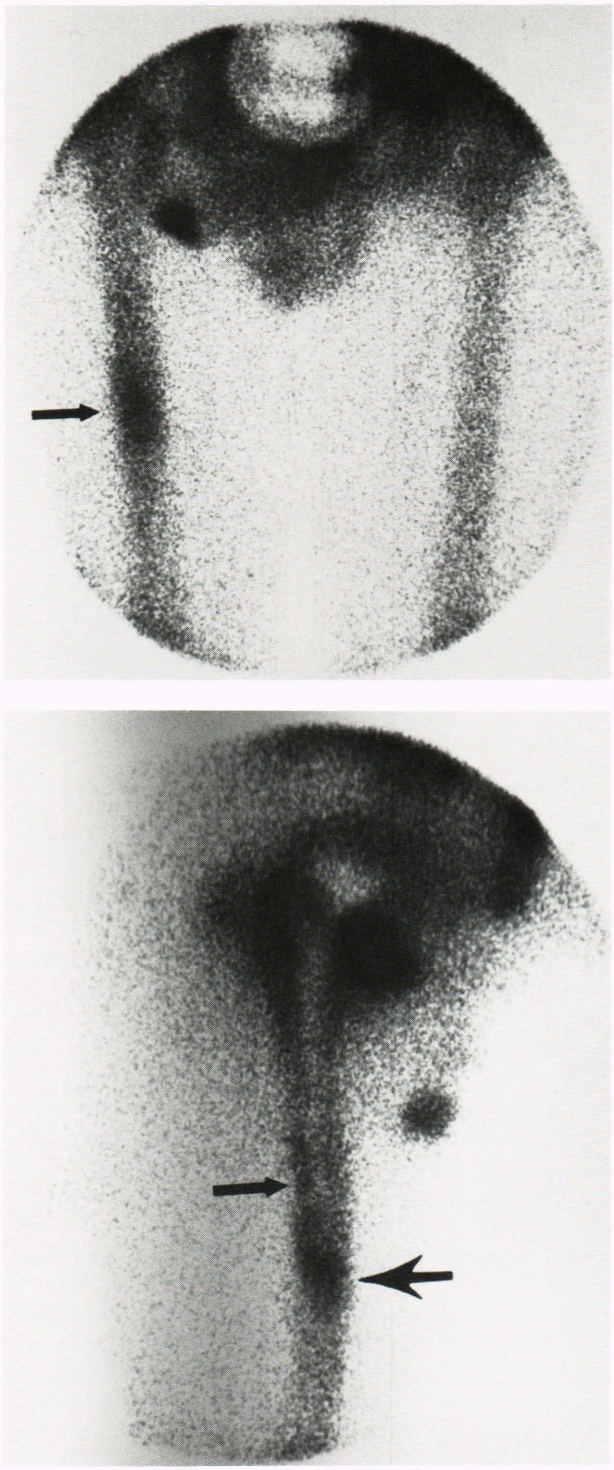

Figure 13. Two views of a technetium bone scan of a patient complaining of midthigh pain. Arrows indicate areas of activity in the vicinity of high stress concentrations. (Reprinted, with permission, from Ref. 16.)

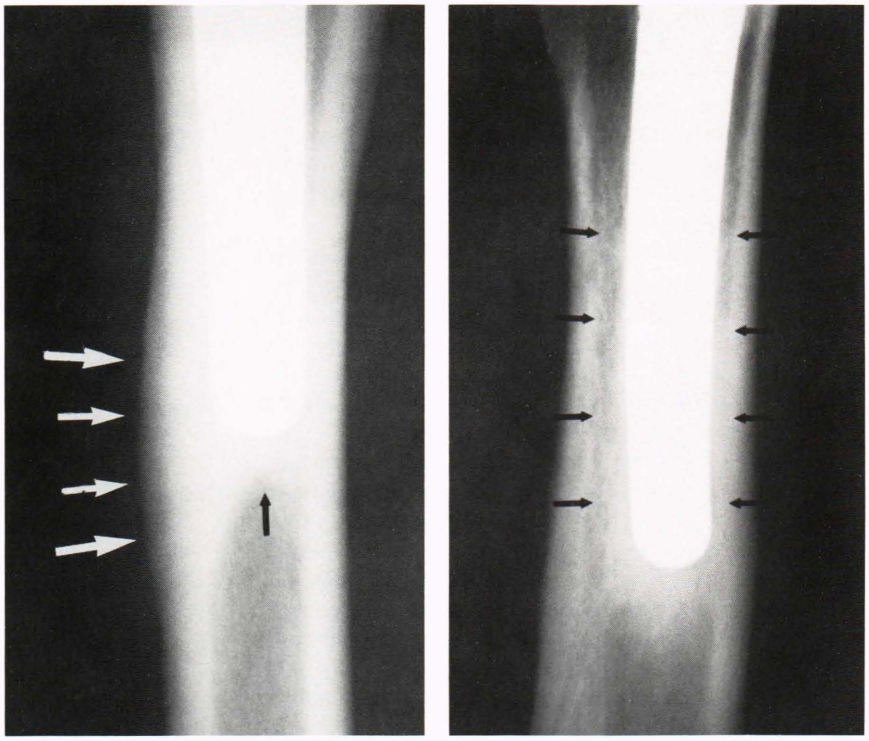

Figure 14. Radiographic changes indicative of bone remodeling. White arrows indicate area of classic cortical hypertrophy; black arrows delineate endosteal consolidation changes. (Reprinted, with permission, from Ref. 16.)

of stress distribution are affected by the stem's length, diameter, rotation (anteversion or retroversion), position (varus [inward angle], valgus [outward angle], neutral), and material properties, and by loading conditions. The dynamic biologic response represents a continuum or gradient of physiologic changes in the mechanical environment, as dictated by the particular situation in question. Although it is unlikely that a single staging or grading system can encompass all these clinical scenarios, a characteristic pattern of physiological remodeling changes probably exists for each clinical situation, secondary to a unique set of stress distributions.

Occasionally, radiographic evidence of tip motion is seen in patients with midthigh pain. A small lucency around the implant tip, often in the presence of endosteal consolidation and cortical hypertrophy, is not uncommon in uncemented total hip replacements.[2] Our study predicts a tendency for the tip to displace radially, secondary to the cantilevering phenomenon that results from the presence of the implant. With proximal biologic or mechanical fixation, the bone/implant complex may remain stable (Fig. 15).

Under physiological loading, both cortical and cancellous bone develop microfractures (Fig. 16), and these bone layers constantly undergo remodeling. This project demonstrates higher than normal peak Hencky–von Mises stress distributions in corresponding locations of previously described radiographic changes in the cortical and cancellous layers. It is conceivable that loads of these magnitudes are responsible for increased frequency of microfractures. As part of the healing process, an increase in trabecular mass occurs through the addition of large quantities of callus. This increase in bone mass effectively stiffens the bone structure. The process may be responsible, in part, for the remodeling of trabecular bone in response to stress.[7–9, 54–56]

Because bone is constantly remodeling itself, and structurally it is a composite of collagen and hydroxyapatite, failure does not occur, even in the presence of microfractures. The ultimate strength of bone is greater than either the collagen or hydroxyapatite alone. In biomechanics course lectures, Y. C. Fung has indicated that the softer (collagen) component prevents the stiffer (hydroxyapatite) component from brittle cracking. Conversely, the stiffer component prevents the soft component from yielding.[57] This complex architecture resists ultimate fatigue failure in the presence of physiological microfractures.

Although to date no clinical or laboratory study has attempted to correlate directly the relationship of midthigh pain to bone remodeling, microfractures, or implant tip motion, the presence of midthigh pain is well documented.[13–17] Whether the pain results from one, all, or a combination of these physiological changes is probably not clinically important. Its existence indicates that nerve fibers in the midthigh area must be activated. Local areas of pressure and stretch secondary to bone remodeling or tip motion, in conjunction with direct mechanical trauma secondary to microfractures (with subsequent callus formation), are responsible for activation of the unmyelinated type-C afferent nerve fibers of the periosteum (the layer of cells at the cortex surface to which soft tissue attaches), osteon, or medullary cavity (Fig. 1).[10,11,58]

Two electron microscopic studies defining osteon morphology, supervised by R. A. Robinson (personal

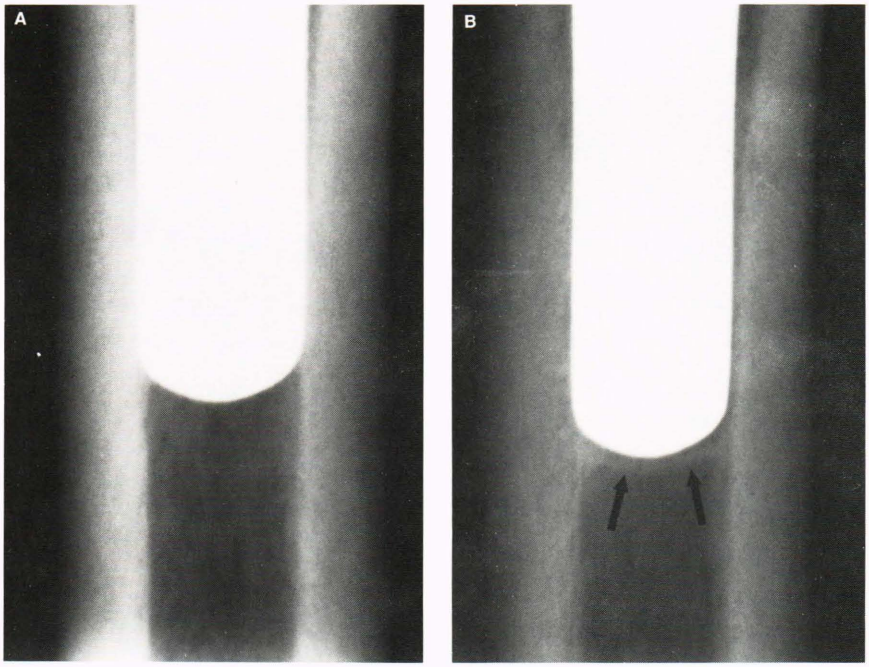

Figure 15. Two serial postoperative X rays. **A**. Six weeks after surgery. **B**. Six months after surgery. These X rays show a thin area of lucency at the implant tip indicative of tip motion. (Reprinted, with permission, from Ref. 16.)

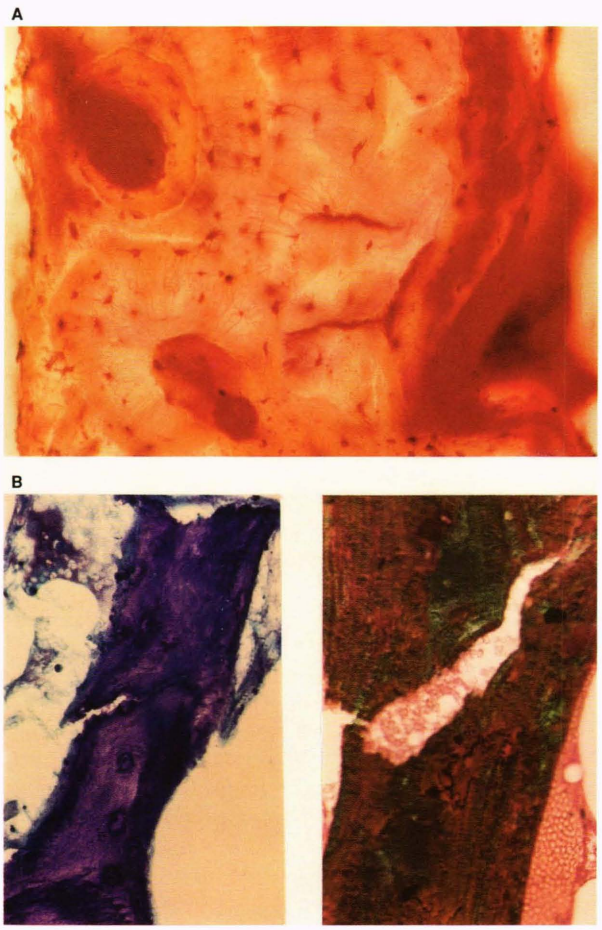

Figure 16. Microscopic photographs of microfractures. **A**. Cortical bone microfractures often found under physiological loading conditions. **B**. Trabecular microfractures. (Photos reprinted, with permission, from A. Villanueva.)

communication, 1989), clearly demonstrated the presence of unmyelinated nerve fibers and Schwann cells in the osteon (Fig. 17). The type-C fibers appeared to adhere to the basement membrane of the microvasculature. Because these nerve fibers are unmyelinated, they have slow conduction velocities (less than 2.0 m/s). The efferent function appears to be autonomic, possibly involved with vasomotor innervation. On the other hand, the afferent conduction pathway senses deep pressure (somatic) and is probably responsible for the diffuse, dull, aching sensation characteristic of midthigh pain.[10,11]

It is not uncommon to see cortical thickening, endosteal consolidation, and tip lucency after midthigh pain has resolved. Presumably, the bone develops a new ultrastructure as an adaptive response to unphysiological stresses transmitted to the adjacent bone. Eventually, bone reaches a new dynamic equilibrium in response to the presence of the implant. As a part of this new steady state, the cortical and cancellous layers increase their stiffness, thereby increasing resistance to local bending and minimizing the potential for local nerve pressure and stretch. The gain in ultimate strength increases resistance to microfractures, thereby minimizing potential for direct mechanical nerve trauma. These various adaptive responses could possibly be responsible for the gradual disappearance of midthigh pain.

CONCLUSIONS

Midthigh pain is an iatrogenic problem of the 1980s that evolved from the advent of uncemented stems with larger diameters and longer lengths. Many of these stiffer stems are currently being cemented, and it remains to be seen whether midthigh pain will become a problem in this patient population.

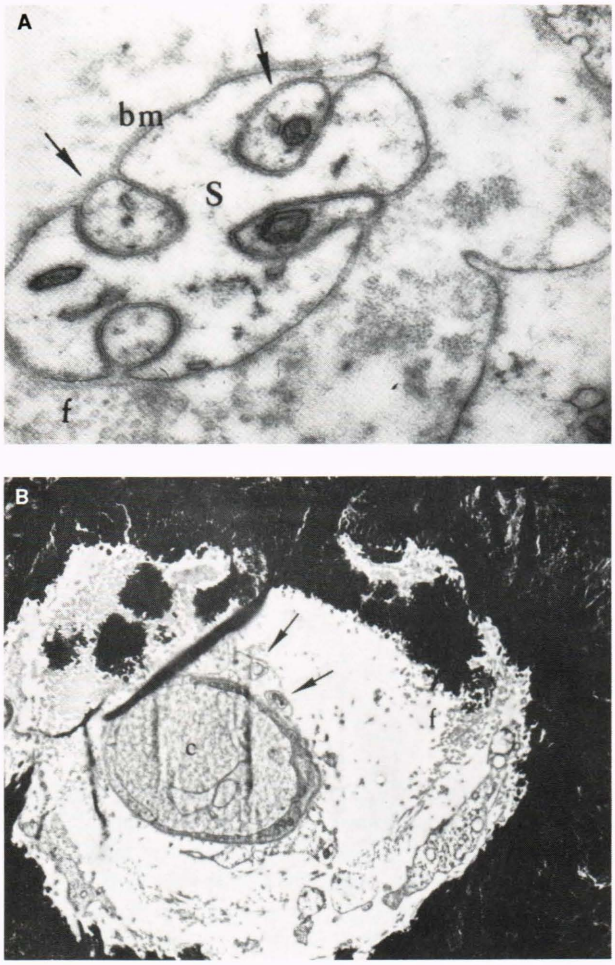

Figure 17. Osteon morphology. **A**. Lead citrate stain (×42,000) of Schwann cell (S) with multiple unmyelinated nerve fibers (f). (bm = basement membrane). **B**. Lead citrate strain (×4,850) of a Haversian canal with single capillary (c) with endothelial lined walls. Adjacent to this vessel is an unmyelinated nerve with two nerve fibers (arrows). (Reprinted, with permission, from Ref. 11.)

This study has clearly shown, for the first time, that there are definite perturbations in the mechanical stresses and strains in the distal cortical and cancellous bone related to different lengths of stem, different implant material properties, and different loading conditions for an uncemented femoral prosthesis. The changes in the stress/strain environment within the femur after total hip arthroplasty have been incorporated into a cascade chart that details the physiological events that result in midthigh pain (Fig. 18).

The solution to preventing midthigh pain in future hip designs is complex. Simply replacing bone with metals, cements, or composite materials is inadequate.[59–62] All those materials have the potential of creating an unphysiological stress environment within the femur. The ideal prosthesis would distribute stresses throughout the bone/implant structure so that the tensile and compressive stress concentrations, along with their corresponding neutral stress plane, behave physiologically.

The domain of orthopedics is rapidly approaching an era that will employ advanced synthetic materials. Computer technology and improved finite-element techniques bring near the potential for optimized artificial hip designs (geometry and material stiffness, for example). Simply reducing the stiffness of an implant to levels similar to cortical bone, however, may still have detrimental physiological effects (midthigh pain) because of high peak cortical stresses. Further analysis of both the proximal and distal areas is required before sufficient data can be generated to develop an optimized geometry and an optimized variable stiffness matrix for hip replacement components of the future.

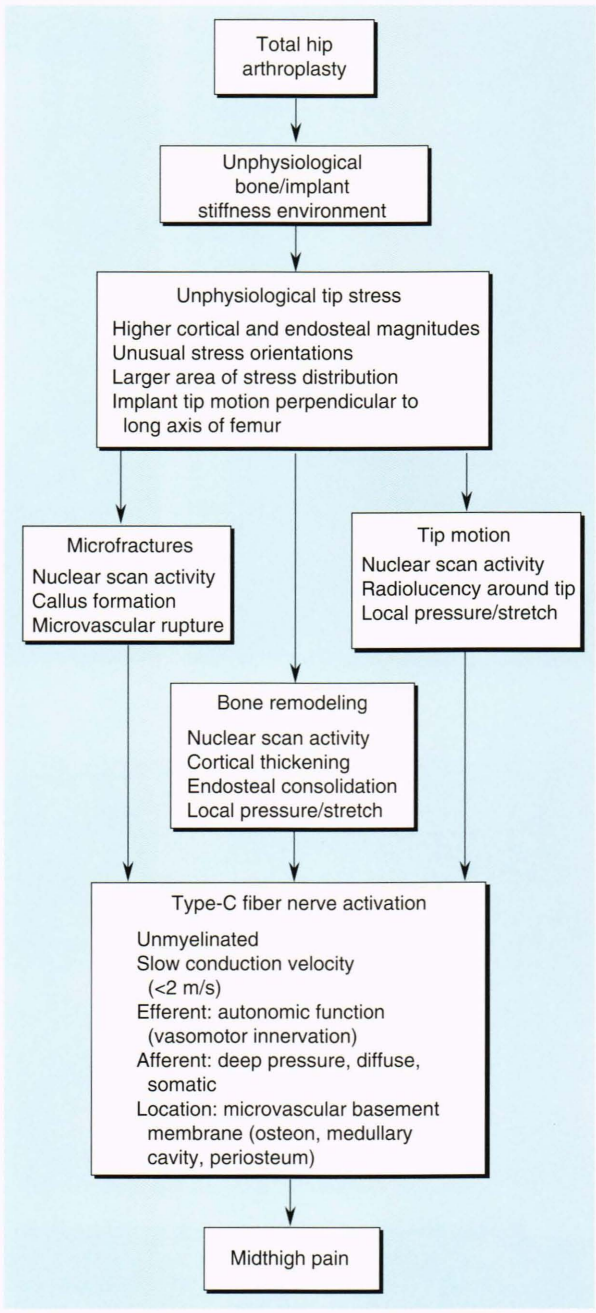

Figure 18. Cascade chart of physiological events resulting in midthigh pain after total hip arthroplasty.

REFERENCES

[1] Engh, C. A., and Balsyn, J. A., *Biological Fixation in Total Hip Arthroplasty*, Slack Inc., Thorofare, N.J., pp. 135–189 (1985).

[2] Gruen, T. A., "Radiographic Criteria for the Clinical Performance of Uncemented Total Joint Replacements," *Quant. Charact. Perform. Porous Implants Hard Tissue Appl.* **953**, 207–218 (1987).

[3] Wolff, J., "Das Gesetz der Transformation der inneren Architektur der Knochen bei, pathologiscen Veranderungen der ausseren Kochenform," *Sitzungsber. Preuss. Akad. Wiss., Phys. Math. Kl.* **22** (1884).

[4] Roux, W., "Gesammelte Abhandlungen über die Entwicklungs-mechanik der Organismen," Bd. I und II, Wilhelm Engelmann, Leipzig (1895).

[5] Kummer, B., "Funktioneller Vau und Funktionelle Anpassing des Knochens," *Anat. Anz.* **111**, 261–293 (1962).

[6] Fyhrie, D. P., and Carter, D. R., "A Unifying Principle Relating Stress to Trabecular Bone Morphology," *J. Orthop. Res.* **4**, 304–317 (1986).

[7] Pugh, J. W., and Rose, R. M., "Mechanical Behavior of Cancellous Bone: A Finite Element Model," in *First New England Conference on Bioengineering*, Pope, M. H., McKay, R. W., and Absher, R. G. (eds.), University of Vermont Department of Electrical Engineering, Burlington, pp. 46–63 (1973).

[8] Pugh, J. W., Rose, R. M., and Radin, E. L., "A Possible Mechanism of Wolff's Law: Trabecular Microfractures," *Arch. Int. Physiol. Biochim.*, **81**(1), 27–40 (1973).

[9] Pugh, J. W., Rose, R. M., and Radin, E. L., "Elastic and Viscoelectric Properties of Trabecular Bone: Dependence on Structure," *J. Biomech.* **6**, 475–485 (1973).

[10] Cooper, R. R., Milgram, J. W., and Robinson, R. A., "Morphology of the Osteon," *J. Bone J. Surg. Am. Vol.* **48-A** (7), 1239–1271 (1986).

[11] Milgram, J. W., and Robinson, R. A., "An Electron Microscopic Demonstration of Unmyelinated Nerves in the Haversian Canals of the Adult Dog," *Bull. Johns Hopkins Hosp.* **117**(3), 163–173 (1965).

[12] Charnley, J., "Arthroplasty of the Hip," *Lancet* **1**, 1129–1132 (1961).

[13] Crenshaw, A. H., *Campbell's Operative Orthopaedics*, C. V. Mosby, St. Louis, Mo., pp. 1246 and 1252 (1987).

[14] Bands, R., Pelker, R. R., Shine, J. J., Bradburn, H. B., Margolis, R. N., et al., "The PCA Hip Prosthesis: A Clinical Followup and X-Ray Analysis of 65 Cases," presented at the 56th annual meeting, American Academy of Orthopaedic Surgeons, Las Vegas, Nev. (11 Feb 1989).

[15] Callaghan, J. J., Dysart, S. H., and Savory, C. G., "The Uncemented Porous-Coated Anatomic Total Hip Prosthesis," *J. Bone J. Surg. Am. Vol.* **70-A**, 337–346 (1988).

[16] Engh, C. A., Bobyn, J. A., and Gorski, J. M., "Biological Fixation of a Modified Moore Prosthesis," *Orthopedics* **7**(2), 285–298 (1984).

[17] Hedley, A. K., Gruen, T. A. W., Borden, L. S., Hungerford, D. S., Habermann, E., et al., "Two-Year Followup of the PCA Noncemented Total Hip Replacement," in *The Hip*, C. V. Mosby, St. Louis, Mo., pp. 225–250 (1986).

[18] Mikhail, W. E., Hoblitzell, R. M., Simpson, J. M., Sabin, J. J., and Ling, R. S., "Comparison of Cemented (Exeter) Vs. Uncemented (P.C.A.) Collarless Femoral Components: 2–5 Year Followup," presented at 55th annual meeting, American Academy of Orthopaedic Surgeons, Atlanta, Ga. (Feb 1988).

[19] Amtmann, E., "The Distribution of Breaking Strength in The Human Femur Shaft," *J. Biomech.* **1**, 271–277 (1968).

[20] Crowninshield, R. D., Brand, R. A., Johnson R. C., and Milroy, J. C., "An Analysis of Femoral Component Stem Design in Total Hip Arthroplasty," *J. Bone J. Surg. Am. Vol.* **62-A** 68–78 (Jan 1980).

[21] Evans, F. G., and Lebow, M., "Directional Differences" in *Mechanical Properties of Bone*, Evans, F. G. (ed.), Charles C. Thomas, Springfield, Ill., pp. 83–121 (1973).

[22] Evans, F. G., and Lebow, M., "Regional Differences in Some of the Physical Properties of the Human Femur," *J. Appl. Physiol.* **3**, 563–572 (1951).

[23] Knauss, P., "Material Properties and Strength Behavior of Spongy Bone Tissue at the Coxal Human Femur," *Biomed. Tech.* **26**, 200–210 (1981).

[24] Lappi, V. G., King, M. D., and LeMay, I., "Determination of Elastic Constraints for Human Femurs," *J. Biomech. Eng.* **101**, 193–197 (Aug 1979).

[25] Rapperport, D. J., Carter, D. R., and Schurman, D. J., "Contact Finite Element Stress Analysis of the Hip Joint," *J. Orthop. Res.* **5**, 548–561 (1985).

[26] Reilly, D. T., Burstein, A. H., and Frankel, V. H., "Elastic Modulus for Bone," *J. Biomech.* **7**, 271–275 (1974).

[27] Vichnin, H. H., and Batterman, S. C., "Stress Analysis and Failure Prediction in the Proximal Femur Before and After Total Hip Replacement," *J. Biomech. Eng.* **108**, 33–41 (1986).

[28] Hodge, W. A., Figan, R. S., Carlson, K. L., Burgess, R. G., Harris, W. H., et al., "Contact Pressures in the Human Hip Joint Measured *In Vivo*," *Proc. Natl. Acad. Sci. U.S.A.* **83**, 2879–2883 (1986).

[29] Bergmann, G., Siraky, J., and Rohlmann, A., "A Comparison of Hip Joint Forces in Sheep, Dog and Man," *J. Biomech.* **17**(12), 907–912 (1984).

[30] Brown, T. D., and DiGioia, A. M., "A Contact-Coupled Finite Element Analysis of the Natural Adult Hip," *J. Biomech.* **17**(6), 437–448 (1984).

[31] Brown, T. D., and Shaw, D. T., "In Vitro Contact Stress Distribution in the Natural Human Hip," *J. Biomech.* **16**(6), 373–384 (1983).

[32] Greenwald, A. S., and O'Connor, J. J., "The Transmission of Load Through the Human Hip Joint," *J. Biomech.* **4**, 507–528 (1971).

[33] Rushfeldt, P. D., Mann, R. W., and Harris, W. H., "Improved Techniques for Measuring In Vitro the Geometry and Pressure Distribution in the Human Acetabulum," *J. Biomech.* **14**(5), 315–323 (1981).

[34] Hansen, T. M., and Koeneman, J. B., "The Use of Structural Partitioning within ANSYS to Solve Nonlinearities within Human Hip Replacement Models," in *ANSYS 1987 Conference Proceedings*, Swanson Analysis Systems, Inc., Houston, Pa., pp. 6.1–6.17, (1987).

[35] Hansen, T. M., and Koeneman, J. B., "To Solve Nonlinearities with Human Hip Replacement Models," *Finite Element News* **4**, 37–41 (1988).

[36] Huiskes, R., and Chao, E. Y. S., "A Survey of Finite Element Analysis in Orthopedic Biomechanics: The First Decade," *J. Biomech.* **16**(6), 385–409 (1983).

[37] Huiskes, R., and Vroeman, W., "A Standardized Finite Element Model for Routine Comparative Evaluations of Femoral Hip Prostheses," *Trans. Annu. Meet. Orthop. Res. Soc.* **10**, 98 (1985).

[38] Koeneman, J. B., and Hansen, T. M., "The Effect of Elastic Modulus, Geometry and Interface Conditions on Bone Stress Around Implants," in *1991 Biomechanics Conference*, Am. Soc. Mech. Eng. Appl. Mech. Dir., **AMD-120**, pp. 117–120 (1991).

[39] Poss, R., Robertson, D. D., Walker, P. S., Reilly, D. T., Ewald, F. C., et al., "Anatomic Stem Design for Press-Fit and Cemented Application," in *Noncemented Total Hip Arthroplasty*, Fitzgerald, R., Jr. (ed.), Raven Press, New York, pp. 343–363 (1988).

[40] Saejong, S., Hirano, S., Granholm, J. W., and Walker, P. S., "The Influence of the Interface on Bone Strains and Stem-Bone Micromotion in Press-Fit Total Hip Stems," *Trans. Annu. Meet. Orthop. Res. Soc.* **12**, 484 (1987).

[41] Basu, P. K., Beall, A. G., Simmons, D. J., and Vannier, M. D., "3-D Femoral Stress Analysis Using CT Scans and P-Version FEM," *Biomater. Med. Devices Artif. Organs* **13**(3,4), 163–186 (1985–1986).

[42] Winget, J. M., "Advanced Graphics Hardware for Finite Elements Results Display," in *Advanced Topics in Finite Element Analysis*, Am. Soc. Mech. Eng. Pressure Vessels Piping Div., New York, **PVP-143**, pp. 53–57 (Jun 1988).

[43] Brown, T. D., Pedersen, D. R., Radin, E. L., and Rose, R. N., "Global Mechanical Consequences of Reduced Cement/Bone Coupling Rigidity in Proximal Femoral Arthroplasty: A Three-Dimensional Finite Element Analysis," *J. Biomech.* **21**(2), 115–129 (1988).

[44] Cezayirlioglu, H., Bahniuk, E., Davy, D. T., and Heiple, K. G., "Anisotropic Yield Behavior of Bone Under Combined Axial Force and Torque," *J. Biomech.* **18**(1), 61–65 (1985).

[45] Koeneman, J. B., and Hansen, T. M., "Finite Element Analysis of a Composite Material Dog Femoral Component," *Trans. Annu. Meet. Orthop. Res. Soc.* **15**, 456 (1990).

[46] Koeneman, J. B., Hansen, T. M., and Weinstein, A. M., "The Effect of Interface Conditions and Implant Design on the Biomechanics of the Proximal Femur," *Trans. Annu. Meet. Orthop. Res. Soc.*, **13**, 526 (1988).

[47] Rohlmann, A., Mossner, V., Bergman, G., Hees, G., and Kolbel, R., "Effects of Stem Design and Material Properties on Stresses in Hip Endoprosthesis," *J. Biomed. Eng.* **9**, 77–83 (1987).

[48] Rohlmann, A., Mossner, V., Bergmann, G., and Kolbel, R., "Finite Element Analysis and Experimental Investigation in a Femur with Hip Endoprosthesis," *J. Biomech.* **16**(9), 727–742 (1983).

[49] Bergmann, G., Graichen, F., Siraky, J., Jendrzynski, H., and Rohlmann, A., "Multichannel Strain Gauge Telemetry for Orthopedic Implants," *J. Biomech.* **21**(2), 169–176 (1988).

[50] Kummer, B., "Photoelastic Studies on the Functional Structure of Bone," *Folia Biotheoretica* **6**, 31–40 (1966).

[51] Wuh, H. C. K., Jones, L. C., and Hungerford, D. S., "Strain Analysis of the Proximal Femur After Total Hip Replacement," *Quant. Charact. Perform. Porous Implants Hard Tissue Appl.* **953**, 249–263 (1987).

[52] Noble, P. C., Kamaric, E., Alexander, J. W., and Tullos, M. S., "What Makes Cementless Implants Work?" presented at the 56th annual meeting, American Academy of Orthopaedic Surgeons, Las Vegas, Nev. (9–14 Feb 1989).

[53] Amtmann, E., *Mechanical Stress, Functional Adaptation and the Variation Structure of the Human Femur Diaphysis*, Springer-Verlag, N.Y., pp. 7–81 (1971).

[54] Carter, D. R., Schwab, G. H., and Spengler, D. M., "Tensile Fracture of Cancellous Bone," *Acta Orthop. Scand.* **51**, 733–741 (1980).

[55] Cowin, S. C., "Wolff's Law of Trabecular Architecture at Remodeling Equilibrium," *J. Biomech. Eng.* **108**, 83–88 (1986).

[56] Stone, J. L., Beaupre, G. S., and Hayes, W. C., "Multiaxial Strength Characteristics of Trabecular Bone," *J. Biomech.* **16**(9), 743–752 (1983).

[57] Fung, Y. C., *Biomechanics, Mechanical Properties of Living Tissue*, Springer-Verlag, N.Y., pp. 383–400 (1981).

[58] Sherman, M. S., "The Nerves of Bone," *J. Bone Joint Surg.* **45-A**(3), 522–528 (1963).

[59] Diegel, P. A., Daniels, A. V., and Dunn, H. K., "Initial Effect of Collarless Stem Stiffness on Femoral Bone Strain," *J. Arthroplasty* **4**(2), 173–178 (1989).

[60] Jamison, R. D., "Fabrication and Characterization of Composite Material Human Hip Prosthesis," presented at the Third Joint ASCE/ASME Mechanics Conference, San Diego, Calif. (9–12 Jul 1989).

[61] Ling, F. F., Roberts, J. C., and Jones, W. R., *Fabrication and Wear Test of a Continuous Fiber/Particulate Composite Total Surface Hip Replacement*, NASA Technical Memorandum 81746, Joint Lubrication Conference, pp. 1–14 (Oct 1981).

[62] Roberts, J. C., and Ling, F. F., "The Design of a Continuous Fiber Composite Surface Hip Replacement," *Trans. ASME J. Mech. Design*, Paper no. 80-CA/DET-29, 1–7 (Feb 1980).

ACKNOWLEDGMENTS: Special thanks to Lee H. Riley, Jr., for support of this research and endless hours of teaching over the past four years and to Robert "Robbie" A. Robinson for personal communication on this topic and years of dedication to the education of orthopedic surgery residents at the Johns Hopkins Hospital. Specimen preparation and finite-element model generation were performed at the following locations: Brigham and Women's Hospital, Boston, Mass.; JHU/Department of Orthopedic Surgery; and JHU/APL. This project was funded by the following institutions and corporations: JHU/APL, JHU/Department of Orthopedic Surgery, the Institute for Bone and Joint Disorders, the Institute for Bioengineering, Silicon Graphics, Inc., Sun Microsystems, Inc., the MacNeal-Schwendler Corporation, PDA Engineering, Inc., Tektronix Corporation, Phoenix Video Group, Manufacturing and Consulting Services, Inc., and A. HOUBERBACKEN. Special thanks to the following individuals for their advice and contributions of clinical photographs, X rays, and slides: Thomas A. Gruen, Lynne C. Jones, David S. Hungerford, Anthony Villanueva, and Anthony K. Hedley. The results of this study were presented previously at the MacNeal-Schwendler Corporation World Users' Conference in March 1990 (Outstanding Paper Award), at the American Society of Mechanical Engineers Computers in Engineering Conference in August 1990 (awards luncheon keynote speaker), at the 1990 summer meeting of the American Hip Society (invited guest of Dr. Phillip Nelson), at the First World Congress of Biomechanics in September 1990, and at the orthopedic grand rounds at Ohio State University and the Johns Hopkins Hospitals. Engineering symposia were presented at Arizona State University, JHU/APL, and Bell Helicopter/TEXTRON.

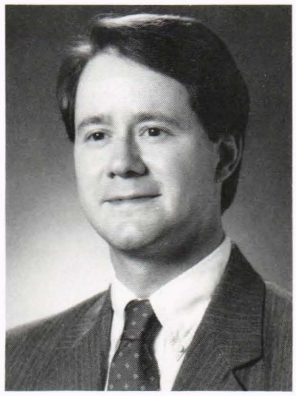

JOHN A. ECKER is a mechanical engineer and a member of the APL Senior Professional Staff. He received a B.S. in mechanical engineering from The Johns Hopkins University and an A.A. in engineering from Hagerstown Junior College. Mr. Ecker was employed with Grove Manufacturing Company in Shady Grove, Pennsylvania, before joining the APL staff in 1983. He has been involved with the use of computer-aided engineering and computer-aided design tools for the design and analysis of mechanical hardware systems. In 1987, Mr. Ecker joined the Aeronautics Department, Engineering Structures Section and has been involved in programs performing structural analyses and programs using advanced composite materials. He is a member of the JHU/APL Biomedical Programs Advisory Committee.

THE AUTHORS

JAMES A. ST. VILLE is an orthopedic surgeon and bioengineer in Phoenix, Arizona. He received an M.D. from the University of Oklahoma and an M.S. in bioengineering from the University of California, San Diego. Dr. St. Ville completed the Halsted general surgery residency and orthopedic surgery residency requirements at the Johns Hopkins Medical Institutions and recently completed a one-year fellowship in artificial joint surgery at the Institute for Bone and Joint Disorders in Phoenix. He is now a practicing physician and bioengineer at the Orthopaedic Bioengineering Institute in Phoenix. Throughout his career, Dr. St. Ville has actively pursued the use of finite-element analysis methods in the improvement of total hip arthroplasty surgical techniques. He was selected keynote speaker at the 1990 American Society for Mechanical Engineers, Computers in Engineering Conference and accepted an award ("in recognition of outstanding contributions to the advancement of computer applications in engineering") on behalf of the authors.

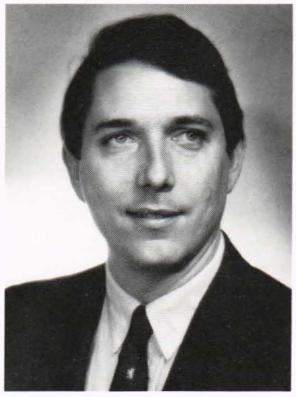

JAMES M. WINGET is a principal scientist in Research and Development at Silicon Graphics, Inc., in Mountain View, California. He received both his Ph.D. and M.S. in applied mechanics from the California Institute of Technology and his B.S. in engineering from the University of Cincinnati. Dr. Winget has consulted on numerous finite-element analysis projects for Lockheed Missiles and Space Company, Inc.; Stanford University; and Sutherland, Sproull and Associates, Inc. He was previously a research assistant professor in biomedical engineering at Duke University and acted as a consultant to the Radiation Oncology Division.

MERI H. BERGHAUER is a medical graphics illustrator in Elm Grove, Wisconsin. She received a B.F.A. from the University of Wisconsin, Milwaukee, and had advanced graphics training at the Milwaukee Area Technical College. She was previously a graphic artist at Northbrook Hospital and Director of Art at DePaul Hospital. Ms. Berghauer assisted in the preparation of the illustrations for this article and was instrumental in the development of a poster version presented at the First World Congress of Biomechanics in 1990.